Research Square

Preprints are preliminary reports that have not undergone peer review.
They should not be considered conclusive, used to inform clinical practice,
or referenced by the media as validated information.

Comparative Deacidification of High Free Fatty Acid Crude Palm Oil Using Activated Carbon, Zeolite, and Calcium-Based Adsorbents

Ratna Sri Harjanti

ratnasriharjanti.yogya@gmail.com

Politeknik LPP Yogyakarta

Muhamad Mustangin

Politeknik LPP Yogyakarta

Research Article

Keywords: crude palm oil, deacidification, free fatty acids, activated carbon, zeolite, calcium carbonate, adsorption kinetics

Posted Date: November 9th, 2026

DOI: https://doi.org/10.21203/rs.3.rs-11411044/v1

License: This work is licensed under a Creative Commons Attribution 4.0 International License.
Read Full License

Additional Declarations: No competing interests reported.

Comparative Deacidification of High Free Fatty Acid Crude Palm Oil Using Activated Carbon, Zeolite, and Calcium-Based Adsorbents

Ratna Sri Harjanti[1,*)], Muhamad Mustangin[2]

[1]*Industrial Chemical Engineering Technology, Politeknik LPP Yogyakarta, Jalan LPP No. 1A, Balapan, 55222 Yogyakarta, Indonesia*
[2]*Plantation Industrial Mechanical Engineering Technology, Politeknik LPP Yogyakarta, Jalan LPP No. 1A, Balapan, 55222 Yogyakarta, Indonesia*

[*)]*Corresponding Author: ratnasriharjanti.yogya@gmail.com*

Abstract

Crude palm oil (CPO) is a promising renewable feedstock for high-value industrial applications; however, its high free fatty acid (FFA) content limits its physicochemical stability and subsequent processing. This study comparatively evaluated activated carbon, zeolite, calcium carbonate ($CaCO_3$), KOH-modified activated carbon, and KOH-modified zeolite for CPO deacidification through contact-time and vacuum–thermal treatments. Material characteristics were examined using SEM, EDX, and FTIR, while time-dependent FFA removal was evaluated using Weber–Morris and Elovich kinetic models. During the five-day treatment, $CaCO_3$ achieved the highest final FFA removal of 47.6%, whereas activated carbon and zeolite reached maximum removals of 43.9% and 40.1%, respectively, on day 4. KOH modification altered material characteristics but did not consistently improve FFA removal. Kinetic analysis revealed material-dependent behavior: KOH-modified activated carbon exhibited the highest apparent Weber–Morris diffusion slope, while unmodified activated carbon showed the strongest agreement with the Elovich model. Under vacuum–thermal treatment at 450 mmHg and 120–180 °C, KOH-modified activated carbon exhibited the strongest temperature-dependent relationship ($R^2 = 0.9356$, $p = 0.0327$), with an apparent $\Delta H°$ of 29.64 kJ mol^{-1}. Overall, CPO deacidification was governed by material characteristics, mass transfer, contact time, and temperature, while KOH modification did not necessarily result in higher FFA removal efficiency.

Keywords: crude palm oil; deacidification; free fatty acids; activated carbon; zeolite; calcium carbonate; adsorption kinetics

1. Introduction

The increasing demand for sustainable and biodegradable industrial materials has encouraged the exploration of renewable vegetable oils as alternatives to petroleum-derived products. Crude palm oil (CPO) is an abundant and economically important vegetable oil with potential applications beyond the food and biodiesel sectors, including biolubricants, hydraulic fluids, and biodegradable insulating oils. However, impurities such as free fatty acids (FFA), moisture,

pigments, phospholipids, and trace metals constrain the direct use of CPO in high-value industrial applications by adversely affecting its physicochemical stability and subsequent processing. Among these impurities, high FFA content is particularly important because it promotes oxidation and corrosion, reduces storage stability, and may compromise the quality of downstream products. Free fatty acid content is an important quality parameter in crude oil processing, and its reduction constitute an important component of oil refining and purification (Lamas, 2022; Zhong et al., 2026) Therefore, effectively reducing CPO acidity is an important pretreatment step for further refining and utilization in higher-value applications (Andari et al., 2023; Bruun et al., 2019; Sitanggang et al., 2020).

Adsorption using solid materials offers an attractive approach to reducing acidity because it is relatively simple to operate and requires limited chemical neutralization. Activated carbon is particularly promising because its porous carbonaceous structure and surface functionalities provide sites for interaction with acidic compounds. Previous studies have demonstrated reductions in oil acidity using activated carbon under different operating conditions (Bavaresco et al., 2021; Bintari, 2019; Buczek & Chwiakowski, 2008). Its adsorption characteristics can be further altered through chemical or thermal activation using agents such as KOH, NaOH, H_3PO_4, and $ZnCl_2$ (Khurshid et al., 2022; Naji & Tye, 2022; Zhang et al., 2015). KOH activation, in particular, has been reported to modify pore development and surface characteristics of carbonaceous materials (Zhang et al., 2015). Recent comparative studies on edible oil purification have also demonstrated that activated carbon and zeolitic materials can reduce FFA content, although their effectiveness varies with adsorbent characteristics and selectivity (Pratama et al., 2026). However, improved structural characteristics after chemical modification do not necessarily guarantee enhanced removal performance in complex oil matrices, and this relationship remains insufficiently understood for high-FFA CPO.

Zeolites represent another potential material for CPO purification because their aluminosilicate framework provides adsorption and ion-exchange properties toward polar compounds and metal species. Zeolite 13X, for example, has been reported to adsorb oleic acid from sunflower oil, while zeolitic materials have also been applied for moisture and metal removal (Erdem et al., 2004; Ilgen & Dulger, 2016; Lestari et al., 2016; Wen et al., 2016). Similar to activated carbon, zeolite properties can be modified through hydrothermal and alkaline treatments that influence its structure and adsorption characteristics (Feijen et al., 1994; Khaleque et al., 2020; Lakiss et al., 2020).

In addition to carbonaceous and aluminosilicate materials, calcium carbonate ($CaCO_3$) provides a chemically distinct approach for FFA removal. Calcium carbonate-based porous materials can accommodate unsaturated fatty acids, including oleic and linoleic acids (Röcker et al., 2021), while interactions between calcium species and free fatty acids may contribute to fatty-acid removal through mechanisms different from conventional physical adsorption (Zijlstra, 2021). The potential role of $CaCO_3$ in oil processing is further supported by Suppes et al. (2001), who demonstrated that calcium carbonate was catalytically active in fats and oils and that free fatty acids did not inhibit its activity. Their results showed substantial FFA reduction and indicated that free fatty acids could be esterified over $CaCO_3$-based catalysts. However, the precise mechanism of $CaCO_3$ remains unresolved and may involve carbonate basicity, surface calcium species, or Lewis acid interactions between calcium ions and carbonyl groups (Suppes et al., 2001). These findings suggest that $CaCO_3$ may reduce FFA through acid–solid interactions and surface-mediated reactions distinct from the predominantly adsorption-

based behavior of activated carbon and zeolite. Consequently, comparing these chemically different materials under identical CPO treatment conditions may provide insight into the relative contributions of surface adsorption, mass transfer, and acid–solid interactions.

Although activated carbon, zeolite, and calcium-based materials have been investigated individually for removing acidic and polar compounds, direct comparisons of these material classes for high-FFA CPO deacidification under identical treatment conditions remain limited. More importantly, it remains unclear whether alkaline modification of activated carbon and zeolite necessarily improves FFA removal compared with their unmodified counterparts. The combined influences of material modification, prolonged contact time, and vacuum–thermal conditions on CPO deacidification have also received limited attention. Furthermore, kinetic and temperature-dependent analyses that can distinguish the removal behavior of carbonaceous, aluminosilicate, and calcium-based materials remain scarce.

Accordingly, this study comparatively evaluates three chemically distinct classes of solid deacidification materials—carbonaceous, aluminosilicate, and calcium-based materials—under both prolonged contact and vacuum–thermal conditions. Particular attention is given to determining whether KOH modification provides a measurable advantage over unmodified activated carbon and zeolite. The experimental results are further interpreted through material characterization, kinetic modeling, and temperature-dependent analysis to distinguish the roles of surface characteristics, mass-transfer behavior, and thermal response in FFA removal.

Therefore, this study aims to compare the effectiveness of activated carbon, zeolite, $CaCO_3$, KOH-modified activated carbon, and KOH-modified zeolite for reducing FFA in CPO and to evaluate the effects of contact time and vacuum–thermal treatment on their deacidification performance. The removal behavior is further examined through morphological and chemical characterization of the carbonaceous and zeolitic materials, kinetic modeling, and temperature-dependent analysis to provide insight into the mechanisms governing FFA reduction by the different materials.

Materials and methods

1. Materials

The crude palm oil (CPO) used in this study was obtained from PT Perkebunan Nusantara VIII, Indonesia. The initial CPO was characterized by a free fatty acid (FFA) content of approximately 16%, a moisture content of 0.2%, and an impurity content of 0.2%. The treatment materials consisted of activated carbon, zeolite, calcium carbonate ($CaCO_3$), KOH-modified activated carbon, and KOH-modified zeolite. Potassium hydroxide (KOH) was used for the chemical modification of activated carbon and zeolite.

2. Preparation of KOH-Modified Activated Carbon and Zeolite

Activated carbon and zeolite were chemically modified using KOH through an immersion treatment, as illustrated in Figure 1. Each material was separately immersed in a 10% KOH solution and stirred for 15 min, followed by a 12 h soaking period. After treatment, the solids were separated by filtration and thoroughly rinsed with distilled water to remove residual KOH. The treated materials were subsequently dried in an oven at 105 °C before use. The

resulting materials are hereafter referred to as KOH-modified activated carbon and KOH-modified zeolite.

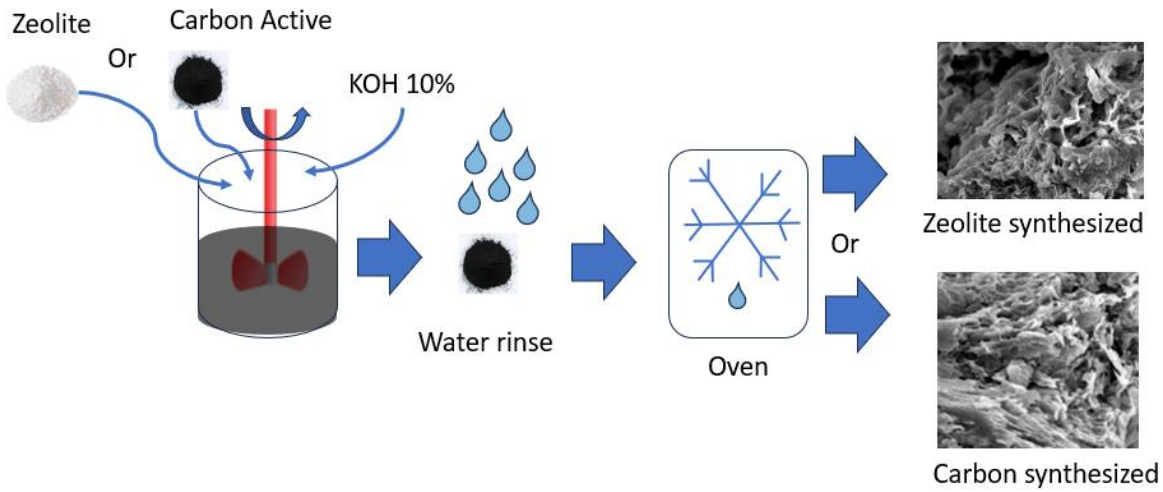


Figure 1. Preparation of KOH-modified activated carbon and zeolite.

Figure 2 depicts the experimental apparatus used for vacuum–thermal treatment of CPO. The setup comprises a vacuum pump with a capability of achieving up to 38 mmHg. A 1000 mL volume of CPO, blended with zeolite, activated carbon, or $CaCO_3$, is heated using an electric heater with a PTC-type temperature sensor. The electric heater, boasting a power capacity of up to 400 W, incorporates a PTC sensor capable of handling temperatures up to 400 °C. The PTC sensor communicates with the temperature controller, signaling it to deactivate the heater once the desired temperature is reached. As the CPO is heated, the vacuum pump concurrently generates vacuum pressure, drawing water vapor or hot air into the tube. To counteract this, the pipe is equipped with a water-cooling system to cool the incoming steam.

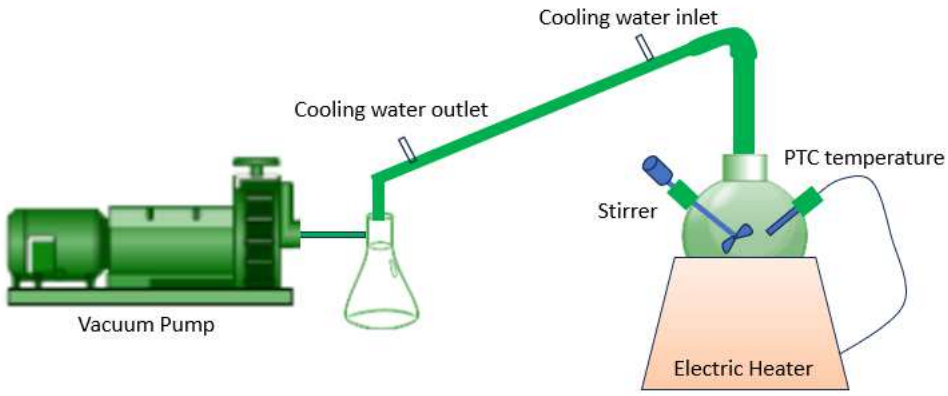


Figure 2. Experimental apparatus for vacuum–thermal treatment of CPO.

The experimental procedure consisted of two deacidification treatments: prolonged contact treatment and vacuum–thermal treatment, as summarized in Figure 3. Five treatment materials

were evaluated: activated carbon, zeolite, $CaCO_3$, KOH-modified activated carbon, and KOH-modified zeolite. In the contact-time experiment, each material was added to CPO at a dosage of 10% (w/w), and the acidity was monitored over a five-day treatment period. In the vacuum–thermal experiment, CPO containing 10% (w/w) of each treatment material was processed under a vacuum pressure of 450 mmHg at temperatures of 120, 140, 160, and 180 °C for 30 min. After thermal treatment, the samples were cooled and filtered to separate the solid material from the treated CPO before acidity measurement.

Activated carbon and zeolite, in both untreated and KOH-modified forms, were additionally characterized by SEM, EDX, and FTIR to evaluate their morphology, elemental composition, and surface chemical characteristics. $CaCO_3$ was included as a calcium-based deacidification material in the performance comparison but was not subjected to the same material characterization. The resulting acidity data were subsequently used to evaluate FFA removal efficiency and to perform kinetic and temperature-dependent analyses.

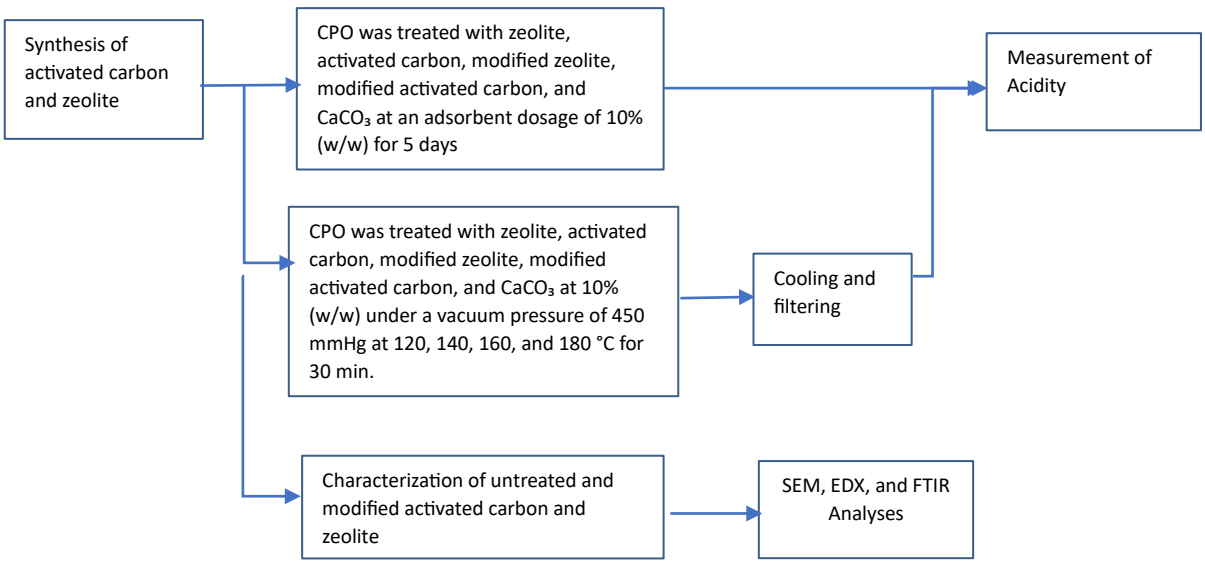


Figure 3. Experimental workflow for CPO deacidification using different treatment materials under contact-time and vacuum–thermal conditions

3. Morphological Measurements

The surface morphology of untreated and KOH-modified activated carbon and zeolite was examined using scanning electron microscopy (SEM) with a JEOL JSM-IT200 instrument (JEOL, Japan). SEM images were acquired at a magnification of 5,000× with a scale bar of 5 µm to evaluate surface morphology, particle structure, and observable micrometer-scale cavities. Elemental composition and spatial elemental distribution were further examined using energy-dispersive X-ray spectroscopy (EDX) and elemental mapping. These analyses were used to evaluate morphological and compositional differences between the untreated and KOH-modified materials.

4. FTIR Measurement

Fourier-transform infrared (FTIR) spectroscopy was used to identify the characteristic functional groups and chemical bonding features of the untreated and KOH-modified activated carbon and zeolite. The spectra were recorded using an IRAffinity-1S FTIR spectrophotometer (Shimadzu, Japan) over a wavenumber range of 400–4000 cm^{-1}. The resulting spectra were interpreted to identify characteristic absorption bands associated with the carbonaceous and aluminosilicate structures and to evaluate possible changes following KOH modification.

5. Acidity measurement

The acidity of untreated and treated CPO samples was determined by titration following the principle of IEC 62021-1. A 5 g oil sample was used for each measurement and titrated with standardized KOH solution. The volume of KOH required to reach the titration endpoint was recorded and used to calculate the acidity, expressed as mg KOH g^{-1} oil, according to Eq. (1)

$$\text{Acidity (mg KOH/g)} = \frac{V \times N \times 56.1}{W} \quad (1)$$

where V is the volume of KOH solution consumed during titration (mL), N is the normality of the KOH solution (mol equivalent L^{-1}), W is the mass of the oil sample (g), and 56.1 is the molecular weight of KOH (g mol^{-1}).

The FFA removal efficiency was calculated relative to the initial acidity of the untreated CPO according to Eq. (2):

$$\text{FFA removal (\%)} = \frac{A_0 - A_t}{A_0} \times 100 \quad (2)$$

where A_o is the initial acidity of untreated CPO and A_t is the acidity after treatment at a given contact time or temperature.

Results and Discussion

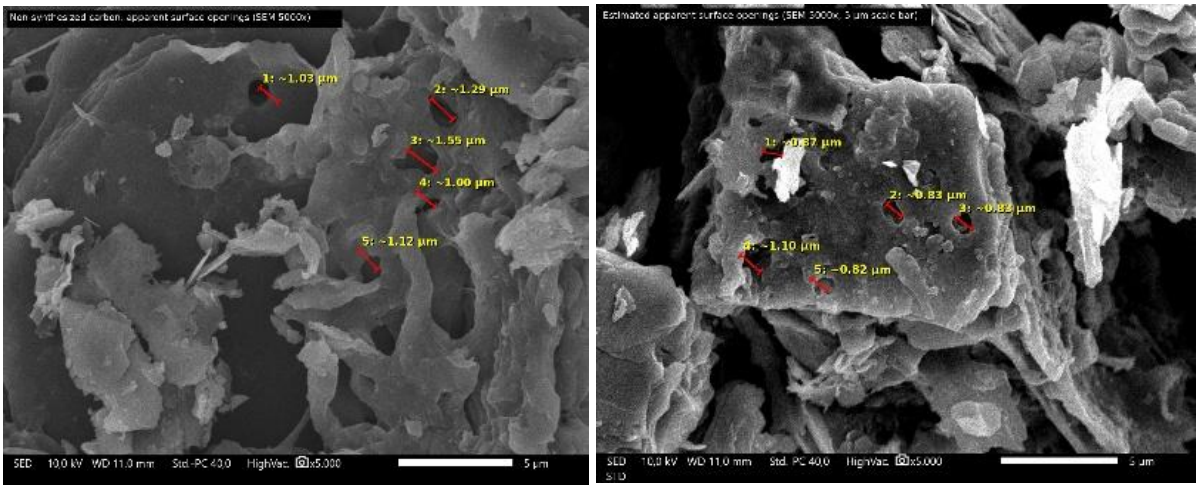
1. Activated Carbon

The surface morphologies of untreated and KOH-modified activated carbon are presented in Figure 4. Both materials exhibited heterogeneous and irregular surface structures, although differences in the morphology of the observable cavities were evident. The untreated activated carbon in Figure 4a showed relatively well-defined surface cavities distributed across the carbonaceous matrix. Image-based estimation of five representative and clearly distinguishable openings indicated apparent cavity sizes of approximately 1.00–1.55 µm, with a mean value of approximately 1.20 µm. In comparison, the KOH-modified activated carbon in Figure 7b exhibited a more fragmented and heterogeneous surface with smaller representative apparent openings of approximately 0.82–1.10 µm and an estimated mean of approximately 0.89 µm. Such heterogeneous surface structures and accessible cavities may provide sites and pathways that facilitate interactions between adsorbate molecules and the carbon surface. Activated carbon has been reported to exhibit adsorption capability associated

with its porous and heterogeneous structure (Belhamdi et al., 2016), while its application to vegetable oils has demonstrated potential for acidity reduction (Bavaresco et al., 2021).

The morphological differences observed after KOH treatment should be interpreted in relation to the relatively mild modification conditions employed in this study. The activated carbon was immersed in 10% KOH and subsequently dried at 105 °C rather than subjected to conventional high-temperature chemical activation. KOH activation is strongly influenced by thermal treatment, and substantial development of porous carbon structures is generally associated with considerably higher activation temperatures (Kaya et al., 2018; Khurshid et al., 2022). Therefore, the smaller apparent cavities observed in the KOH-modified sample should not be interpreted as evidence that KOH modification inherently decreases the intrinsic pore size. Instead, the SEM observations suggest that low-temperature KOH treatment altered the external morphology without producing the extensive pore development typically associated with high-temperature activation. This may partly explain why KOH modification did not consistently improve FFA removal compared with untreated activated carbon.

It should be emphasized that the dimensions estimated from Figure 4 represent apparent micrometer-scale surface cavities observable at 5,000× magnification rather than intrinsic pore diameters. Therefore, these measurements cannot be used to characterize micropore or mesopore distributions. Quantitative determination of specific surface area, pore volume, and pore-size distribution would require dedicated analyses such as N_2 adsorption–desorption and BET measurements. Nevertheless, the SEM observations provide morphological evidence of differences between untreated and KOH-modified activated carbon and complement the adsorption behavior observed during CPO deacidification.



(a) (b)

Figure 4. SEM micrographs of (a) untreated activated carbon and (b) KOH-modified activated carbon at 5,000× magnification, showing representative micrometer-scale surface cavities.

EDX Analysis of KOH-Modified Activated Carbon

EDX analysis of the KOH-modified activated carbon showed that the analyzed surface was predominantly composed of carbon (84.52 mass%), followed by oxygen (8.41 mass%),

potassium (3.98 mass%), aluminum (1.93 mass%), and silicon (1.15 mass%). Elemental mapping further showed that carbon was widely distributed throughout the analyzed region, whereas O, K, Al, and Si occurred at substantially lower intensities and exhibited more localized distributions in Figure 5. The high carbon content is consistent with the carbonaceous nature of the material, while the presence of oxygen indicates oxygen-containing surface species that may contribute to interactions with polar components such as FFA. The detected potassium is also consistent with the use of KOH during the modification process and may represent residual potassium-containing species associated with the treated carbon surface.
Because EDX data for the untreated activated carbon were not available, the present elemental analysis cannot quantitatively establish compositional changes resulting from KOH modification. Accordingly, the EDX results are interpreted primarily as characterization of the elemental composition of the KOH-modified activated carbon rather than direct evidence of modification-induced elemental changes. Possible changes in surface functional groups were further evaluated by FTIR analysis.

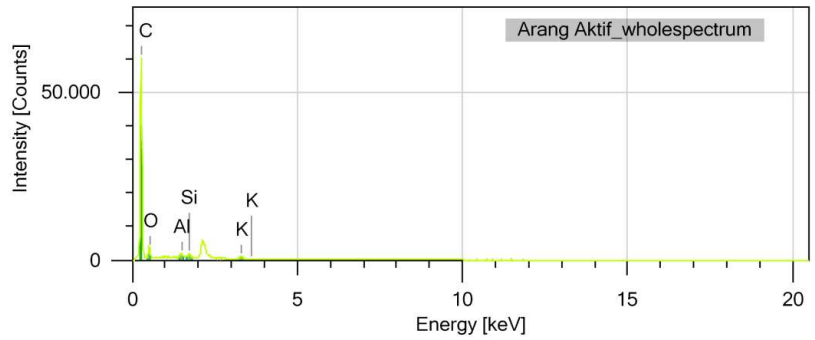


Figure 5. EDX analysis of KOH-modified activated carbon

FTIR Analysis of KOH-Modified Activated Carbon

Figure 6 presents the FTIR spectrum of the KOH-modified activated carbon. The spectrum shows broad absorption features over the investigated wavenumber range, indicating the presence of chemically heterogeneous surface functionalities on the carbonaceous material. The spectral profile, particularly toward the fingerprint region, is consistent with the presence of oxygen-containing functionalities commonly reported on activated carbon surfaces (Endes Yılmaz et al., 2023; Rodrigues et al., 2020). This interpretation is also qualitatively consistent with the EDX results, which confirmed the presence of oxygen in the KOH-modified activated carbon. Oxygen-containing surface functionalities are relevant to adsorption because they may influence the polarity and chemical interaction of the carbon surface with adsorbate molecules. However, the individual absorption bands in the present spectrum were not sufficiently resolved to permit reliable assignment of specific functional groups. Although absorption features in similar spectral regions have previously been attributed to oxygen-containing bonds such as C–O and C–O–C in carbonaceous materials (Li et al., 2019), assigning individual functional groups solely from the present spectrum would be speculative. Furthermore, because an FTIR spectrum of the untreated activated carbon was not available, modification-induced changes in surface functional groups cannot be directly established. Therefore, the FTIR result is interpreted primarily as complementary characterization of the KOH-modified activated carbon rather than direct evidence of a specific chemical mechanism for FFA removal. Together with SEM and EDX, the FTIR analysis indicates that the modified carbon

possesses heterogeneous morphological and chemical surface characteristics that may contribute to its interaction with FFA during CPO deacidification.

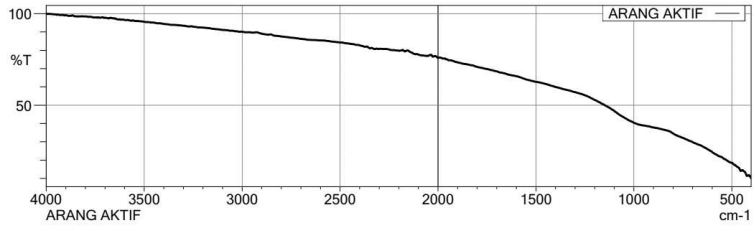


Figure 6. FTIR spectrum of KOH-modified activated carbon

2. Zeolite

The surface morphologies of untreated and KOH-modified zeolite are presented in Figure 7. The untreated zeolite in Figure 7 (a) exhibited a heterogeneous morphology consisting predominantly of irregular and angular particles with rough surfaces and substantial particle agglomeration. Based on the SEM scale, the observable particle fragments were approximately 0.2–5 μm in size, with most individual fragments occurring within approximately 0.5–2 μm. Interparticle voids and micrometer-scale surface cavities were also observed between the aggregated particles. These morphological features may provide accessible external surfaces and diffusion pathways for interactions between FFA molecules and the zeolite material. However, the observed cavities should not be interpreted as the intrinsic micropore size of zeolite, because such pores are below the direct resolution applicable to the present SEM morphological assessment.

The KOH-modified zeolite in Figure 7 (b) also exhibited an irregular and heterogeneous morphology, with aggregated particles and observable surface cavities. Representative apparent cavity openings in the selected SEM region ranged from approximately 0.85 to 1.05 μm, with a mean value of approximately 0.92 μm. This value was comparable to the representative cavities observed in the untreated zeolite (approximately 0.89 μm), suggesting that the KOH treatment employed in this study did not produce a substantial enlargement of the micrometer-scale surface openings observable by SEM. Therefore, the morphological observations do not provide evidence that the low-temperature KOH treatment substantially increased the intrinsic porosity of the zeolite.

This result should be interpreted in relation to the relatively mild modification procedure used in the present study, in which zeolite was treated with 10% KOH and subsequently dried at 105 °C. Zeolite modification involving alkaline or hydrothermal treatment is commonly influenced by hydrothermal conditions, temperature, alkalinity, and treatment time (Khaleque et al., 2020; Lakiss et al., 2020). Consequently, the present low-temperature treatment may have modified the external surface morphology and surface chemistry without extensively restructuring the zeolite framework. This interpretation is consistent with the comparable apparent cavity dimensions observed before and after KOH treatment. It may partly explain

why KOH modification did not consistently enhance FFA removal compared with untreated zeolite. Quantitative confirmation of changes in specific surface area, pore volume, and intrinsic micro-/mesopore distribution would require complementary characterization such as N_2 adsorption–desorption/BET analysis.

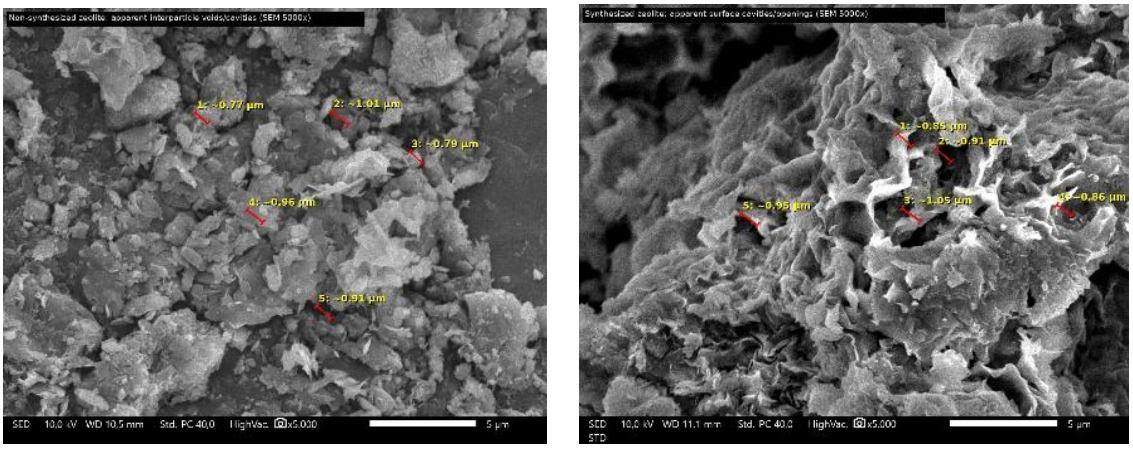


Figure 7. SEM micrographs of (a) untreated zeolite and (b) KOH-modified zeolite at 5,000× magnification, showing representative micrometer-scale surface features.

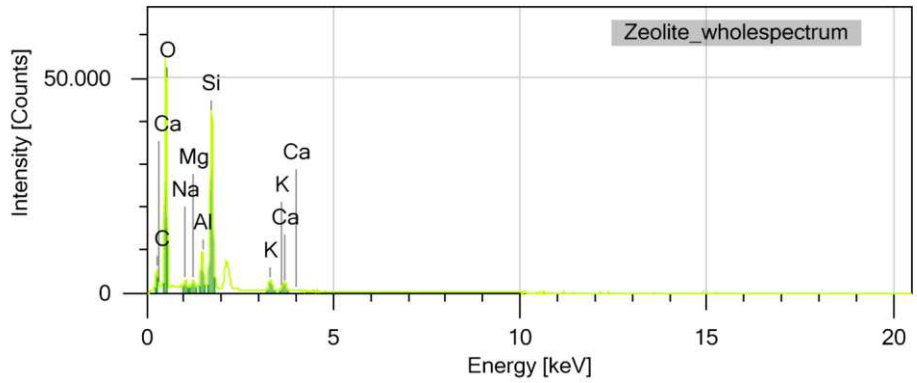


Figure 8. EDX analysis of KOH-modified zeolite

The elemental composition and spatial distribution of the KOH-modified zeolite were further evaluated by EDX analysis and elemental mapping in figure8. The EDX spectrum revealed O and Si as the predominant elements, accounting for 39.20 and 32.06 wt.%, respectively, followed by C (8.66 wt.%), K (6.90 wt.%), Ca (5.78 wt.%), and Al (5.61 wt.%), with smaller amounts of Na (0.93 wt.%) and Mg (0.86 wt.%). Based on the atomic compositions of Si (23.21 at.%) and Al (4.23 at.%), the Si/Al atomic ratio was approximately 5.49, indicating a relatively Si-rich aluminosilicate composition. Elemental mapping further showed that Si, O, and Al were broadly distributed throughout the analyzed surface, supporting the aluminosilicate-rich character of the material, whereas Ca and other minor elements exhibited comparatively heterogeneous distributions. The detection of K is also consistent with the use of KOH during the modification process.

The aluminosilicate-rich composition together with the presence of mineral cations such as K, Ca, Na, and Mg indicates a chemically heterogeneous surface that may provide interaction sites for polar compounds, including FFA. However, because corresponding EDX data for the untreated zeolite were not available, the present elemental analysis cannot quantitatively establish compositional changes induced by KOH modification. Therefore, the EDX results are interpreted primarily as characterization of the elemental composition of the KOH-modified zeolite rather than direct evidence of modification-induced elemental changes.

Notably, the KOH-modified zeolite did not exhibit markedly superior FFA-removal performance compared with the untreated zeolite. This observation is consistent with the SEM results, which showed relatively comparable apparent micrometer-scale surface openings before and after modification. Taken together, the SEM and EDX results suggest that the mild KOH treatment produced a material with heterogeneous morphological and chemical characteristics, but these characteristics did not translate into a substantial improvement in FFA-removal performance under the conditions investigated in this study.

The FTIR spectrum of the KOH-modified zeolite is presented in Figure 9. A prominent absorption band at approximately 1002.98 cm^{-1} was observed and can be attributed to asymmetric stretching vibrations of Si–O–Si and Si–O–Al bonds within the aluminosilicate framework. Similar bands in this spectral region have been reported for different zeolitic materials (Ng et al., 2019; Safak Boroglu & Ali Gurkaynak, 2011). The band at approximately 790.81 cm^{-1} can be associated with symmetric vibrations of the silicate framework, while the bands at approximately 583.63 and 509.23 cm^{-1} are attributable to framework vibrations involving Si–O and Al–O structural units (Mozgawa et al., 2011; Ng et al., 2019). Collectively, these absorption features are consistent with the characteristic aluminosilicate structure of zeolitic materials.

In the higher-wavenumber region, the weak band at approximately 3614.60 cm^{-1} is associated with surface hydroxyl groups, whereas the feature at approximately 1627.92 cm^{-1} may be attributed to bending vibrations of adsorbed water associated with the zeolite surface (Chakarova & Hadjiivanov, 2013; Yu et al., 2014). A weaker feature was also observed at approximately 1427.32 cm^{-1}; however, its assignment should be interpreted cautiously because FTIR alone is insufficient to identify the specific surface species responsible for this band.

The FTIR observations are consistent with the EDX results, which identified Si, O, and Al as the principal framework-forming elements and yielded a Si/Al atomic ratio of approximately 5.49. Together, FTIR and EDX therefore support the aluminosilicate character of the KOH-modified zeolite. However, because corresponding FTIR data for the untreated zeolite were not available, changes in functional groups or framework chemistry induced specifically by KOH modification cannot be directly established. Accordingly, the FTIR results are interpreted primarily as structural characterization of the KOH-modified zeolite rather than direct evidence of modification-induced chemical changes.

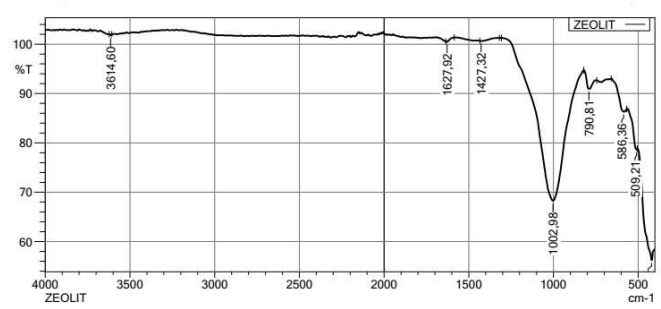
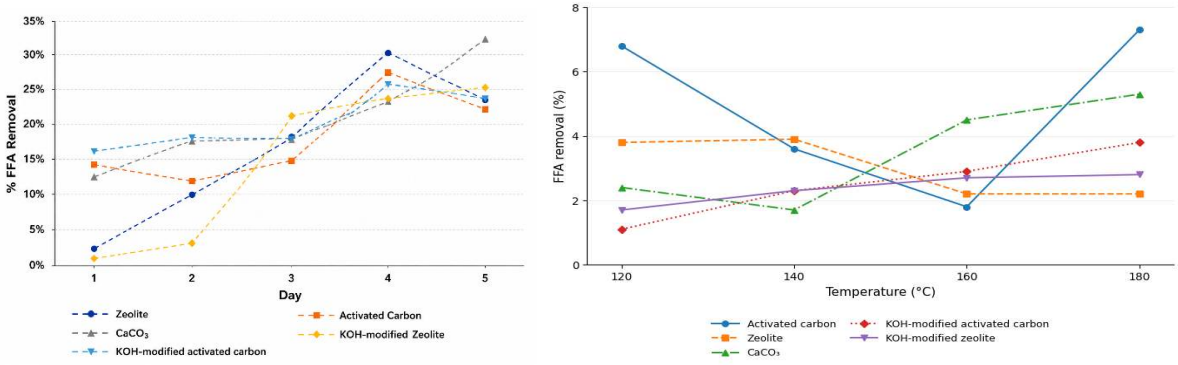


Figure 9. FTIR analysis of KOH-modified zeolite

The relevance of surface chemistry to FFA removal showed that surface modification altered the membrane's affinity for FFA during CPO deacidification, indicating that FFA removal may depend not only on morphology but also on specific interactions between FFA and surface functional groups (Azmi et al., 2015).

Figure 10(a) presents the effect of contact time on FFA removal during the five-day treatment. FFA removal generally increased with contact time, although the response differed among the materials. $CaCO_3$ showed the highest removal at the end of the treatment period, whereas activated carbon and zeolite reached their maximum removal on day 4. Figure 10(b) shows the effect of temperature on FFA removal under vacuum–thermal treatment at 450 mmHg. The temperature response was strongly material dependent, and increasing temperature did not consistently enhance FFA removal across all materials.

Table 1 presents the corresponding FFA removal efficiencies, further demonstrating the differences among the treatment materials. $CaCO_3$ showed the highest final FFA removal after prolonged contact, while activated carbon and zeolite reached their maximum removal earlier in the treatment period. Interestingly, KOH modification did not consistently improve the performance of either activated carbon or zeolite compared with their untreated forms. These results indicate that CPO deacidification depends on the treatment conditions as well as the characteristics and interaction behavior of the materials.



(a). .. (b)

Figure 10. %FFA removal (a). Effect of contact time and material type (b). Effect of temperature and material type under vacuum–thermal treatment

Table 1. %FFA Removal of CPO

Day	Carbon (%)	Zeolite (%)	$CaCO_3$ (%)	KOH-modified activated carbon (%)	KOH-modified zeolite (%)
1	2.1	21.1	19.2	1.1	23.7
2	15.0	17.9	26.1	4.5	26.9
3	27.1	21.9	26.3	30.9	26.3
4	43.9	40.1	35.1	34.4	40.4
5	35.7	33.4	47.6	36.3	33.9

3. Kinetic Calculation Mechanism and Rationale for Weber-Morris and Elovich Models

The time-dependent behavior of free fatty acid (FFA) removal was further evaluated using two non-equilibrium kinetic models, namely the Weber–Morris intraparticle diffusion model and the Elovich equation. The Weber–Morris model was evaluated according to Eq. (3):

$$q_t = K_{id} t^{0.5} + C \tag{3}$$

where qt represents the FFA removal (%) at contact time, (K_{id}) represents the apparent intraparticle diffusion rate constant, and C is associated with the contribution of boundary-layer effects. The Elovich model was evaluated using Eq. (4):

$$q_t = \frac{1}{\beta} ln\,(\alpha\beta) + \frac{1}{\beta} ln(t) \tag{4}$$

where (α) represents the initial adsorption rate and $(\beta)$is related to the variation in adsorption energy and surface coverage.

These models were selected as complementary approaches after the conventional pseudo-first-order (PFO) and pseudo-second-order (PSO) models produced unrealistically high predicted equilibrium adsorption capacities relative to the experimentally observed values, indicating that these conventional models did not adequately describe the five-day FFA removal behavior. The Weber–Morris model was therefore employed to assess the possible contribution of intraparticle diffusion and boundary-layer mass transfer to the observed removal process. In parallel, the Elovich model was applied to evaluate whether the time-dependent FFA removal behavior was consistent with adsorption on energetically heterogeneous surfaces and adsorbent–adsorbate interactions. Because only five contact-time observations were available, these models were used as an exploratory kinetic assessment rather than as definitive evidence of a single rate-controlling mechanism.

Table 2. Weber–Morris and Elovich kinetic parameters for FFA removal

	Day	Carbon	Zeolite	$CaCO_3$	KOH-modified activated carbon	KOH-modified zeolite
Data %FFA Removal	1	2.1	21.1	19.2	1.1	23.7
	2	15.0	17.9	26.1	4.5	26.9
	3	27.1	21.9	26.3	30.9	26.3
	4	43.9	40.1	35.1	34.4	40.4
	5	35.7	33.4	47.6	36.3	33.9
Weber - Morris	K_{id}	0.03	14.66	20.72	33.00	11.03
	C	0.99	2.29	-3.88	-33.88	11.72
	R^2	0.88	0.57	0.85	0.87	0.62
	P value (intercept)	0.09	0.87	0.68	0.07	0.27
	P value (slope)	0.02	0.14	0.03	0.02	0.11
Elovich	1/β	24.71	10.58	15.18	25.11	8.28
	Intercept	1.11	16.73	16.32	-2.60	22.29
	R^2	0.90	0.51	0.78	0.86	0.59
	P value (intercept)	0.85	0.09	0.05	0.71	0.01
	P value (slope)	0.01	0.18	0.05	0.02	0.13

Kinetic assessment using the Weber–Morris intraparticle diffusion and Elovich models provided complementary insights into the time-dependent FFA removal behavior of the investigated adsorbents as summarized in Table 2. KOH-modified activated carbon exhibited the highest apparent Weber–Morris diffusion slope (K_{id} = 33.00). However, its large negative intercept indicates that the Weber–Morris relationship should not be interpreted as evidence of intraparticle diffusion as the sole rate-controlling mechanism. Instead, the relatively high linearity (R^2 = 0.87) suggests a strong time-dependent diffusion response within the investigated contact period. A comparable behavior was the adsorption of minor components from crude palm oil onto acid-activated bleaching earth under high-temperature and low-pressure conditions (Silva et al., 2013). Their intraparticle diffusion analysis indicated that intraparticle diffusion contributed to the adsorption process but was not the sole rate-limiting step. This observation supports the present interpretation that the relatively strong Weber–Morris relationship reflects a diffusion-related contribution rather than a single controlling mechanism. Previous studies using the Weber–Morris approach have also shown that deviations from an origin-intersecting relationship indicate that boundary-layer or film diffusion may contribute alongside intraparticle diffusion (Santos et al., 2025). A similar engineering approach was adopted by for the adsorption of carotenoids from hybrid palm oil, where contact time, temperature, adsorption kinetics, intraparticle diffusion, and thermodynamic parameters were jointly evaluated to understand the adsorption process (Vidoca et al., 2020). Although the target compound and adsorbent differed from those investigated in the present study, their results demonstrate that adsorption behavior in palm-oil systems is governed by the combined effects of mass transfer, adsorbent characteristics, and temperature rather than by adsorption capacity alone. This supports the present approach of interpreting FFA removal through complementary kinetic, material-characterization, and temperature-dependent analyses. Recent reassessment of the Weber–Morris model has

cautioned against assigning direct mechanistic meaning to the intercept or using deviation from the origin as definitive evidence of additional mass-transfer resistance (Chu et al., 2025). This interpretation is also consistent with recent FFA adsorption studies in oil systems. (Yuniarto et al., 2026) reported that intraparticle diffusion contributed significantly to the mass transfer of FFA from used cooking oil onto biochar-based adsorbents, while additional mass-transfer analysis showed that internal diffusion played an important role in the overall adsorption process (Jafar et al., 2015). Thus, the present results suggest that KOH-modified activated carbon exhibits a strong diffusion-related response, although multiple mass-transfer steps are likely involved.

In contrast, unmodified activated carbon showed the strongest agreement with the Elovich model (R^2=0.90, p = 0.01), indicating that its FFA removal behavior is consistent with adsorption on an energetically heterogeneous surface. The Elovich model is commonly associated with adsorption processes occurring on heterogeneous surfaces in which adsorption energy changes progressively with surface coverage. A comparable interpretation has been reported for fatty-acid adsorption, where the Elovich model satisfactorily described palmitic acid adsorption and attributed it to strong adsorbent–adsorbate interactions (Abdul Manas et al., 2023). However, in the present study, the Elovich fit should be interpreted as evidence of heterogeneous surface interaction rather than definitive proof of chemisorption, particularly because only five contact-time observations were available.

For $CaCO_3$, the Weber–Morris model showed relatively high linearity (R^2=0.85, p = 0.03), suggesting that intraparticle or pore-related mass transfer may contribute to the observed FFA removal. Previous studies of FFA adsorption in oil systems have similarly demonstrated that intraparticle diffusion can contribute to the overall mass-transfer process in porous adsorbents (Yuniarto et al., 2026). However, because the adsorbent characteristics differ from those of $CaCO_3$, this comparison should be regarded as supporting evidence for the possible role of diffusion rather than evidence of an identical mechanism. In the present $CaCO_3$ system, surface-mediated acid–solid interactions may also contribute to FFA removal, and therefore the Weber–Morris relationship should be regarded as evidence of a mass-transfer contribution rather than a complete mechanistic description. In comparison, both untreated and KOH-modified zeolites exhibited weaker linear relationships with the Weber–Morris and Elovich models, indicating that neither single kinetic model adequately represents their time-dependent FFA removal behavior over the five-day contact period. This may reflect the involvement of multiple mass-transfer and surface-interaction processes. This behavior is comparable to observations reported for zeolitic adsorbents, where adsorption may proceed through sequential stages involving external-film transport, intraparticle diffusion, and eventual equilibrium rather than a single rate-controlling mechanism (Santos et al., 2025).

Overall, the kinetic analysis revealed distinct time-dependent behaviors among the investigated adsorbents rather than a single universal adsorption mechanism. KOH-modified activated carbon exhibited the highest apparent Weber–Morris diffusion slope, whereas $CaCO_3$ combined a relatively strong Weber–Morris relationship with the highest observed FFA removal at the end of the five-day treatment. Unmodified activated carbon showed the strongest agreement with the Elovich model, indicating behavior consistent with adsorption on a heterogeneous surface. These findings agree with previous adsorption studies showing that FFA removal may involve simultaneous contributions from external mass transfer, intraparticle diffusion, and heterogeneous surface interactions rather than a single kinetic pathway (Yuniarto

et al., 2026). Therefore, adsorption rate, final FFA removal efficiency, and kinetic-model conformity should be considered separately when evaluating adsorbent performance. Given the limited number of contact-time observations, these kinetic results are interpreted as exploratory evidence of possible mass-transfer and surface-interaction mechanisms rather than definitive identification of a single rate-controlling step.

The contribution of mass-transfer phenomena to FFA removal from vegetable oils has been investigated by FFA adsorption from soybean oil using a strong anion-exchange resin (Deboni et al., 2015). Their kinetic analysis incorporated the Weber–Morris model together with conventional adsorption models, while equilibrium experiments at different temperatures were used to derive thermodynamic parameters. Although the adsorbent chemistry differed from that of the present materials, their study confirms that FFA deacidification in a non-aqueous vegetable-oil matrix can involve coupled adsorption, diffusion, and temperature-dependent phenomena.

The temperature dependence of FFA removal was evaluated under a constant vacuum pressure of 450 mmHg over a temperature range of 120–180 °C. To quantitatively assess each adsorbent's temperature response, a Van't Hoff analysis was performed by establishing a linear relationship between the distribution coefficient (K_d) and reciprocal absolute temperature (1/T). The relationship was expressed according to Eq. (5):

$$\ln K_d = -\frac{(\Delta H^\circ)}{(R)}\left(\frac{(1)}{(T)}\right) + \frac{(\Delta S^\circ)}{(R)} \qquad (5)$$

where K_d is the distribution coefficient, T is the absolute temperature (K), and R is the universal gas constant (8.314 J mol^{-1} K^{-1}). The apparent enthalpy change (ΔH°) and entropy change (ΔS°) were estimated from the slope and intercept, respectively. The coefficient of determination (R^2) and regression p-values were additionally used to evaluate the strength and statistical significance of the temperature-dependent relationship for each adsorbent.

Table 3. Van't Hoff regression parameters for ln Kd versus T^{-1}

Temperature (°C)	Temperature 1/T (K^{-1})	Carbon	Zeolite	$CaCO_3$	KOH-modified activated carbon	KOH-modified zeolite
120	0.002543558	-2.61861	-3.23245	-3.73247	-4.47904	-4.063977692
140	0.002420428	-3.27777	-3.21048	-4.06398	-3.73247	-3.732471534
160	0.002308669	-4.01628	-3.806	-3.04908	-3.50934	-3.599262537
180	0.002206775	-2.54426	-3.806	-2.89198	-3.23245	-3.568433301
Slope (-ΔH°/R)		635.2097	2057.138	-3102.13	-3565.57	-1466.408984
Intercept (Δs°/R)		-4.61959	-8.38886	3.917233	4.711564	-0.265855679
R^2		0.018036	0.780577	0.65409	0.935565	0.879198188
P value (intercept)		0.616449	0.044452	0.409501	0.095437	0.79814773
P value (slope)		0.865702	0.116498	0.191242	0.032754	0.062344313

The Van't Hoff regression parameters for the five adsorbents are summarized in Table 3. The results demonstrate markedly different temperature-dependent behaviors among the investigated materials. KOH-modified activated carbon exhibited the strongest linear relationship between ln Kd and 1/T (R^2 = 0.9356, p = 0.0327), with a negative slope corresponding to an apparent positive enthalpy change (ΔH°) of approximately 29.64 kJ mol^{-1}. This result indicates that FFA removal by KOH-modified activated carbon became increasingly favorable with increasing temperature within the investigated range. KOH-modified zeolite showed a similar apparent endothermic tendency (ΔH° ≈ 12.19 kJ mol^{-1}) and relatively high linearity (R^2 = 0.8792); however, the temperature dependence did not reach statistical significance at $p < 0.05$ (p = 0.0623).

$CaCO_3$ also exhibited an apparent endothermic response, with an estimated ΔH° of approximately 25.79 kJ mol^{-1}. Nevertheless, its moderate linearity (R^2 = 0.6541) and non-significant slope (p = 0.1912) indicate that this thermodynamic interpretation should be treated cautiously. In contrast, unmodified zeolite showed an apparent exothermic tendency (ΔH° ≈ −17.10 kJ mol^{-1}), although its temperature dependence was not statistically significant (R^2 = 0.7806, p = 0.1165). Unmodified activated carbon exhibited the weakest Van't Hoff relationship (R^2 = 0.0180, p = 0.8657), indicating that its response to temperature could not be adequately represented by a simple linear Van't Hoff relationship.

Overall, Table 3 indicates that surface modification altered the temperature response of the investigated adsorbents, with the clearest effect observed for activated carbon. Among the investigated materials, KOH-modified activated carbon showed the strongest temperature-dependent relationship, whereas unmodified activated carbon exhibited no clear linear Van't Hoff response. Although the magnitude of the apparent enthalpy changes was relatively moderate, these values alone are insufficient to assign the FFA removal mechanism exclusively to either physisorption or chemisorption. Therefore, the apparent thermodynamic behavior should be interpreted together with the kinetic results and SEM, EDX, and FTIR characterization to obtain a more comprehensive understanding of the possible deacidification mechanisms.

The observed morphological differences suggest that the KOH-modified treatment altered the surface architecture of activated carbon rather than simply enlarging the visible pores. The smaller apparent openings of the KOH-modified material may reflect surface restructuring, fragmentation, or redistribution of accessible cavities following chemical treatment. Interestingly, this morphological alteration is consistent with the different kinetic behaviors observed for the two carbon materials. KOH-modified activated carbon exhibited the highest apparent Weber–Morris diffusion slope (K_{id} = 33.00), suggesting a stronger time-dependent mass-transfer response, whereas unmodified activated carbon showed the strongest agreement with the Elovich model (R^2 = 0.8970, p = 0.0145), indicating adsorption behavior consistent with an energetically heterogeneous surface. Therefore, the larger visible surface openings observed in the unmodified carbon should not be interpreted as evidence of superior adsorption performance, since FFA removal is likely governed by a combination of accessible surface structure, internal porosity, surface chemistry, and adsorbate–adsorbent interactions.

In contrast, improved FFA removal from CPO was observed after alkaline modification of a dolomite-based adsorbent, which was associated with increased pore size, basic strength, and available basic sites. Notably, their adsorbent underwent high-temperature calcination, whereas

the present KOH modification was conducted under relatively mild thermal conditions, suggesting that, under the conditions investigated here, mild chemical treatment alone may be insufficient to develop the adsorption structures associated with improved FFA removal (Nor Shafizah et al., 2022).

Accordingly, the SEM and kinetic results collectively indicate that KOH modification altered the adsorption environment of activated carbon without necessarily increasing its visible micrometer-scale pore-opening size. This finding emphasizes that apparent surface morphology and kinetic response provide complementary information: SEM describes the accessible external structure, whereas the Weber–Morris and Elovich analyses reflect different aspects of the time-dependent mass-transfer and surface-interaction processes involved in FFA removal.

Future studies should therefore investigate higher-temperature thermal or hydrothermal activation and systematically optimize activation temperature, KOH concentration, and treatment duration. Surface-area and pore-size characterization, particularly through N_2 adsorption–desorption and BET analysis, is also required to establish clearer relationships between adsorbent structure, mass-transfer behavior, and CPO deacidification performance.

Conclusion

This study demonstrates that CPO deacidification effectiveness depends not only on the material used but also on contact time, mass-transfer behavior, and treatment temperature. KOH modification altered the characteristics and kinetic behavior of activated carbon and zeolite but did not consistently enhance their FFA removal performance, indicating that chemical modification alone does not necessarily improve deacidification efficiency. The kinetic analysis further suggests that FFA removal involves material-dependent mechanisms, including diffusion and interactions with heterogeneous surface sites, rather than a single universal adsorption mechanism. $CaCO_3$ showed promising performance during prolonged treatment, while KOH-modified activated carbon exhibited a stronger response to temperature under vacuum–thermal conditions. Overall, the findings highlight the importance of matching material characteristics and processing conditions when designing an effective CPO deacidification process.

Statements and Declarations

This research was funded by the authors themselves. No external funding was received.

REFERENCES

Abdul Manas, N. H., Kumar, N. K. M. F., Mohd Shah, N. A., Ling, G. Y., Azelee, N. I. W., Fuzi, S. F. Z. M., Masngut, N., Bunyamin, M. A. H., Illias, R. M., & El Enshasy, H. A. (2023). Adsorption of Fatty Acid on Beta-Cyclodextrin Functionalized Cellulose Nanofiber. *Sustainability (Switzerland)* , *15*(2). https://doi.org/10.3390/su15021559

Andari, F., Kittel, J., Ropital, F., Fernandes, J., & Dodelin, L. (2023). Corrosion Issues in the Conversion of Vegetable and Waste Oils to Produce Biofuels. In *AMPP Annual Conference + Expo* (p. AMPP-2023-19308).

Azmi, R. A., Goh, P. S., Ismail, A. F., Lau, W. J., Ng, B. C., Othman, N. H., Noor, A. M., & Yusoff, M. S. A. (2015). Deacidification of crude palm oil using PVA-crosslinked PVDF membrane. *Journal of Food Engineering*, *166*, 165–173. https://doi.org/10.1016/j.jfoodeng.2015.06.001

Bavaresco, A., Fonseca, J. M., Scheufele, F. B., da Silva, C., & Teleken, J. G. (2021). Use of carbonized corn cob biomass to reduce acidity of residual frying oil. *Acta Scientiarum - Technology*, *43*, 1–18. https://doi.org/10.4025/actascitechnol.v43i1.51303

Belhamdi, B., Merzougui, Z., Trari, M., & Addoun, A. (2016). A kinetic, equilibrium and thermodynamic study of L-phenylalanine adsorption using activated carbon based on agricultural waste (date stones). *Journal of Applied Research and Technology*, *14*(5), 354–366. https://doi.org/10.1016/j.jart.2016.08.004

Bintari, A. (2019). *Activated Carbon-Based Bio-Adsorbent for Reducing Free*. *050004*(2018).

Bruun, N., Demesa, A. G., Tesfaye, F., Hemming, J., & Hupa, L. (2019). Factors affecting the corrosive behavior of used cooking oils and a non-edible fish oil that are in contact with ferrous metals. *Energies*, *12*(24). https://doi.org/10.3390/en12244812

Buczek, B., & Chwiakowski, W. (2008). *Purification of the used palm oil by adsorption*. (April), 8–11. https://doi.org/10.2478/v10026-008-0005-7

Chakarova, K., & Hadjiivanov, K. (2013). FTIR study of N2 and CO adsorption on H-D-FER. *Microporous and Mesoporous Materials*, *177*, 59–65. https://doi.org/10.1016/j.micromeso.2013.04.022

Chu, K. H., Hashim, M. A., Zawawi, M. H., & Bollinger, J. C. (2025). The Weber-Morris model in water contaminant adsorption: Shattering long-standing misconceptions. *Journal of Environmental Chemical Engineering*, *13*(4), 117266. https://doi.org/10.1016/j.jece.2025.117266

Deboni, T. M., Batista, E. A. C., & Meirelles, A. J. A. (2015). Equilibrium, Kinetics, and Thermodynamics of Soybean Oil Deacidification Using a Strong Anion Exchange Resin. *Industrial and Engineering Chemistry Research*, *54*(44), 11167–11179. https://doi.org/10.1021/acs.iecr.5b02653

Endes Yılmaz, C., Nostar Aslan, E., Aslani, M. A. A., Altaş, Y., & Kütahyalı Aslani, C. (2023). Hydrothermal synthesis of novel activated carbon–nickel oxide nanocomposites for uranium adsorption. *Journal of Radioanalytical and Nuclear Chemistry*, *332*(11), 4791–4805. https://doi.org/10.1007/s10967-023-09006-z

Erdem, E., Karapinar, N., & Donat, R. (2004). The removal of heavy metal cations by natural zeolites. *Journal of Colloid and Interface Science*, *280*(2), 309–314. https://doi.org/10.1016/j.jcis.2004.08.028

Feijen, E. J. P., Martens, J. A., & Jacobs, P. A. (1994). Zeolites and their Mechanism of Synthesis. In J. Weitkamp, H. G. Karge, H. Pfeifer, & W. B. T.-S. in S. S. and C. Hölderich (Eds.), *Zeolites and Related Microporous Materials: State of the Art 1994 - Proceedings of the 10th International Zeolite Conference, Garmisch-Partenkirchen, Germany, 17-22 July 1994* (Vol. 84, pp. 3–21). Elsevier. https://doi.org/https://doi.org/10.1016/S0167-2991(08)64074-4

Ilgen, O., & Dulger, H. S. (2016). Removal of oleic acid from sunflower oil on zeolite 13X: Kinetics, equilibrium and thermodynamic studies. *Industrial Crops and Products*, *81*, 66–71. https://doi.org/https://doi.org/10.1016/j.indcrop.2015.11.050

Jafar, B. M., Hamadneh, I., Khalili, F. I., & Al-dujaili, A. H. (2015). Kinetic Study on Adsorption of Fatty HydroxamicAcids by Natural Clays. *Jordan Journal of Earth and Environmental Sciences*, *7*(1), 11–17.

Kaya, M., Azahin, Ö., & Saka, C. (2018). Preparation and TG/DTG, FT-IR, SEM, BET Surface Area, Iodine Number and Methylene Blue Number Analysis of Activated Carbon from Pistachio Shells by Chemical Activation. *International Journal of Chemical Reactor Engineering*, *16*(2). https://doi.org/10.1515/ijcre-2017-0060

Khaleque, A., Alam, M. M., Hoque, M., Mondal, S., Haider, J. Bin, Xu, B., Johir, M. A. H., Karmakar, A. K., Zhou, J. L., Ahmed, M. B., & Moni, M. A. (2020). Zeolite synthesis from low-cost materials and environmental applications: A review. *Environmental Advances*, *2*(October). https://doi.org/10.1016/j.envadv.2020.100019

Khurshid, H., Mustafa, M. R. U., & Isa, M. H. (2022). Modified Activated Carbon Synthesized from Oil Palm Leaves Waste as a Novel Green Adsorbent for Chemical Oxygen Demand in Produced Water. *Sustainability (Switzerland)*, *14*(4). https://doi.org/10.3390/su14041986

Lakiss, L., Gilson, J.-P., Valtchev, V., Mintova, S., Vicente, A., Vimont, A., Bedard, R., Abdo, S., & Bricker, J. (2020). Zeolites in a good shape: Catalyst forming by extrusion modifies their performances. *Microporous and Mesoporous Materials*, *299*, 110114. https://doi.org/https://doi.org/10.1016/j.micromeso.2020.110114

Lamas, D. L. (2022). Effect of enzymatic degumming process on the physicochemical and nutritional properties of fish byproducts oil. *Applied Food Research*, *2*(2). https://doi.org/10.1016/j.afres.2022.100170

Lestari, D. Y., Purwanigsih, D., & Wiyarsi, A. (2016). Indonesian natural zeolites as potential adsorbent in waste cooking oil regeneration. *Applied Clay Sciences*, *74*(May), 121–126.

Li, F., Katz, L., & Hu, Z. (2019). Adsorption of Major Nitrogen-Containing Components in Microalgal Bio-Oil by Activated Carbon: Equilibrium, Kinetics, and Ideal Adsorbed Solution Theory (IAST) Model. *ACS Sustainable Chemistry and Engineering*, 16529–16538. https://doi.org/10.1021/acssuschemeng.9b03804

Mozgawa, W., Król, M., & Barczyk, K. (2011). FT-IR studies of zeolites from different structural groups. *Chemik*, *65*(7), 671–674.

Naji, S. Z., & Tye, C. T. (2022). A review of the synthesis of activated carbon for biodiesel production: Precursor, preparation, and modification. *Energy Conversion and Management: X*, *13*, 100152. https://doi.org/10.1016/j.ecmx.2021.100152

Ng, T. Y. S., Chew, T. L., Yeong, Y. F., Jawad, Z. A., & Ho, C. D. (2019). Zeolite RHO Synthesis Accelerated by Ultrasonic Irradiation Treatment. *Scientific Reports*, *9*(1), 1–11. https://doi.org/10.1038/s41598-019-51460-x

Nor Shafizah, I., Irmawati, R., Omar, H., Yahaya, M., & Alia Aina, A. (2022). Removal of free fatty acid (FFA) in crude palm oil (CPO) using potassium oxide/dolomite as an adsorbent: Optimization by Taguchi method. *Food Chemistry*, *373*, 131668. https://doi.org/https://doi.org/10.1016/j.foodchem.2021.131668

Pratama, Y., Afidah, U., Zahra, A. T., Saputra, Y. A., Mulyani, S., Ni'matullah Al-Baarri, A., & Simone, E. (2026). Selective adsorbent performance in bleaching black soldier fly larvae oil: Effects on physicochemical and sensory quality. *Applied Food Research*, *6*(2). https://doi.org/10.1016/j.afres.2026.102368

Röcker, B., Mäder, G., Monnard, F. W., Jancikova, M., Welker, M., Schoelkopf, J., & Yildirim, S. (2021). Evaluation of the potential of modified calcium carbonate as a carrier for unsaturated fatty acids in oxygen scavenging applications. *Materials*, *14*(17). https://doi.org/10.3390/ma14175000

Rodrigues, C. V, Santana, K. O., Nespeca, M. G., & ... (2020). Energy valorization of crude glycerol and sanitary sewage in hydrogen generation by biological processes. *International Journal of …*.

Safak Boroglu, M., & Ali Gurkaynak, M. (2011). Fabrication and characterization of silica modified polyimide-zeolite mixed matrix membranes for gas separation properties. *Polymer Bulletin*, *66*(4), 463–478. https://doi.org/10.1007/s00289-010-0286-x

Santos, M. G. dos, Paquini, L. D., Quintela, P. H. L., Profeti, L. P. R., & Guimaraes, D. (2025). Insights into Kinetics and Thermodynamics for Adsorption Methylene Blue Using Ecofriendly Zeolites Materials. *ACS Omega*, *10*(20), 20326–20340. https://doi.org/10.1021/acsomega.4c11718

Silva, S. M., Sampaio, K. A., Ceriani, R., Verhé, R., Stevens, C., De Greyt, W., & Meirelles, A. J. A. (2013). Adsorption of carotenes and phosphorus from palm oil onto acid activated bleaching earth: Equilibrium, kinetics and thermodynamics. *Journal of Food Engineering*, *118*(4), 341–349. https://doi.org/10.1016/j.jfoodeng.2013.04.026

Sitanggang, A., Isharyadi, F., Faridah, D., & Andarwulan, N. (2020). *Physicochemical Characterization of Crude Palm Oil (CPO) in Sumatra and Non Sumatra Region*. (October), 43–48. https://doi.org/10.5220/0009978000430048

Suppes, G. J., Bockwinkel, K., Lucas, S., Botts, J. B., Mason, M. H., & Heppert, J. A. (2001). Calcium carbonate catalyzed alcoholysis of fats and oils. *JAOCS, Journal of the American Oil Chemists' Society*, *78*(2), 139–145. https://doi.org/10.1007/s11746-001-0234-y

Vidoca, L. P., Almeida, E. S. de, Cardoso, M. F., Otavio, L., Valadares, L. F., & Monteiro, S. (2020). Extraction of carotene from crude hybrid palm oil using polymeric resin. *Journal of Food Engineering*, *278*(January), 109944. https://doi.org/10.1016/j.jfoodeng.2020.109944

Wen, J., Yi, Y., & Zeng, G. (2016). Effects of modi fi ed zeolite on the removal and stabilization of heavy metals in contaminated lake sediment using BCR sequential extraction. *Journal of Environmental Management*, *178*, 63–69. https://doi.org/10.1016/j.jenvman.2016.04.046

Yu, Y., Shapter, J. G., Popelka-Filcoff, R., Bennett, J. W., & Ellis, A. V. (2014). Copper removal using bio-inspired polydopamine coated natural zeolites. *Journal of Hazardous Materials*, *273*(December 2018), 174–182. https://doi.org/10.1016/j.jhazmat.2014.03.048

Yuniarto, A., Wijayanti, A. A., & Fulazzaky, M. A. (2026). Isotherm, kinetic, and mass-transfer analysis of free fatty acid adsorption using wood twig-derived biochar and biochar-bentonite composite adsorbents. *Chemical Engineering Journal Advances*, *27*(July), 101349. https://doi.org/10.1016/j.ceja.2026.101349

Zhang, D., Yin, J., Zhao, J., Zhu, H., & Wang, C. (2015). Adsorption and removal of tetracycline from water by petroleum coke-derived highly porous activated carbon. *Journal of Environmental Chemical Engineering*, *3*(3), 1504–1512. https://doi.org/https://doi.org/10.1016/j.jece.2015.05.014

Zhong, W., Li, M. J., Liu, D., Ding, Y. P., Xiang, X. R., Gao, P., Yin, J. J., Wang, S., Yang, Y., He, B., & He, D. P. (2026). Changes in quality parameters at the various stages of arachidonic acid-rich oil refining. *Applied Food Research*, *6*(1). https://doi.org/10.1016/j.afres.2026.101703

Zijlstra, R. T. (2021). Binding Fatty Acids into Indigestible Calcium Soap: Removing a Piece of Pie. *Journal of Nutrition*, *151*(5), 1053–1054. https://doi.org/10.1093/jn/nxab045